analytical chemistry

pubs.acs.org/ac Article

Electrochemical Improvements Can Be Realized via Shortening of the Length of Screen-Printed Electrochemical Platforms

Matthew J. Whittingham, Nicholas J. Hurst, Robert D. Crapnell, Alejandro Garcia-Miranda Ferrari, Elias Blanco, Trevor J. Davies, and Craig E. Banks*

Cite This: https://doi.org/10.1021/acs.analchem.1c03601 Read Online

ACCESS | Metrics & More | Article Recommendations | Supporting Information

ABSTRACT: Screen-printed electrodes (SPEs) are ubiquitous within the field of electrochemistry and are commonplace within the arsenal of electrochemists. Their popularity stems from their reproducibility, versatility, and extremely low-cost production, allowing their utilization as single-shot electrodes and thus removing the need for tedious electrode pretreatments. Many SPE studies have explored changing the working electrode composition and/or size to benefit the researcher's specific applications. In this paper, we explore a critical parameter of SPEs that is often overlooked; namely, we explore changing the length of the SPE connections. We provide evidence of resistance changes through altering the connection length to the working electrode through theoretical calculations, multimeter measurements, and electrochemical impedance spectroscopy (EIS). We demonstrate that changing the physical length of SPE connections gives rise to more accurate heterogeneous electrode kinetics, which cannot be overcome simply through IR compensation. Significant improvements are observed when utilized as the basis of electrochemical sensing platforms for sodium nitrite, β-nicotinamide adenine dinucleotide (NADH), and lead (II). This work has a significant impact upon the field of SPEs and highlights the need for researchers to characterize and define their specific electrode performance. Without such fundamental characterization as the length and resistance of the SPE used, direct comparisons between two different systems for similar applications are obsolete. We therefore suggest that, when using SPEs in the future, experimentalists report the length of the working electrode connection alongside the measured resistance (multimeter or EIS) to facilitate this standardization across the field.

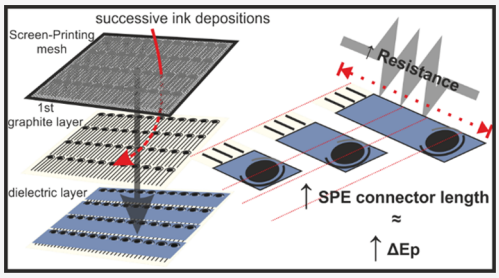

■ INTRODUCTION

Screen-printed electrodes (SPEs) are ubiquitous within the field of electrochemistry and are a principal item within the electrochemists' arsenal of electrodes. This is due to their low cost, versatility, and high reproducibility, allowing a single sensor to be used in each measurement, eliminating the need for electrode pretreatment, and requiring only a few microliters of the sample being interrogated. Due to these inherent advantages, SPEs are particularly favored in electroanalysis[1−4] and allow one to bridge the gap between the laboratory and in-the-field.[5] Screen-printed electrodes are produced by spreading a thixotropic fluid evenly across a mesh screen that defines the geometry of the desired electrode. The thixotropic fluid or ink can contain a variety of substances such as graphite, carbon black, solvents, and polymeric binder where the mesh screen is a negative of the desired shape or electrode.[6−12] Complete SPEs are then manufactured using various screens to build up the desired designs, typically including a reference electrode with Ag/AgCl paste and a dielectric layer to define the electrode areas in contact with the solution. Screen-printed electrodes are versatile, with the design and composition readily changeable for the intended application. In the latter case, SPEs were originally fabricated as carbon/graphite based electrochemical platforms[6] but have been adapted and extended to provide a wide range of electrode surfaces/compositions, *e.g.*, Pt,[13] Au,[14,15] Pd,[16] Cu,[17,18] Ag,[19] carbon nanotubes,[20] graphene,[21] graphene oxide,[22] and bismuth oxide,[23] to name just a few. In the former case, a range of geometries have been realized such as microbands,[24−26] ultramicrobands,[27] microband electrode arrays,[28] microdisc arrays,[29] microelectrodes and microelectrode arrays,[30] and back-to-back configurations,[31] highlighting the versatility of the SPE production methodology. SPEs are used extensively in the production of sensing platforms, with examples ranging from ions[32−34] and small molecules[13,35,36] to larger biological analytes such as proteins.[37−39] They have even been utilized outside of electrochemical sensing platforms due to their large surface area, ease of modification, disposability, and low cost.[40−44] As such, it is critical that SPEs can be reliably compared between different reported works.

Received: August 21, 2021
Accepted: November 18, 2021

In standard three-electrode configuration ohmic drop is an important parameter for experimentalists when performing cyclic voltammetry and other electrochemical methods.[45] *Ohmic drop*, ohmic polarization, or IR drop is the resistance of the media during the flow of electrical current through the cell.[46] According to Ohm's law, the current passed (i) multiplied by the resistance (R_u) equals the potential difference due to ohmic drop. Ohmic drop is referred to as the rate of electrons flowing between electrodes and is related to the amount of current, conductivity of the supporting electrolyte, geometry of the electrodes, and distance between them. The electrochemical cell has an intrinsic resistance (R_c). R_c is made by the combination of the solution resistance (R_{sol}) and the uncompensated resistance between the working and reference electrode (R_u). Ohmic drop is the difference between the potential that is experienced by the analyte in the solution due to R_u and the potential that the equipment actually measures. It can be corrected by positive feedback compensation, mathematical, or computational manipulation of the data, which are often included in the potentiostat's software. Also, note that any resistance within the working electrode will also influence the ohmic drop (*i.e.,* wires, semiconductor materials, resistive films, etc.).[47] For most cases, these compensating mechanisms will reduce ohmic drop until its effect is negligible; however, this manuscript will investigate the influence of the resistance of the working electrode's circuit resistance (between the SPE's WE and its connector) measured by a multimeter, the full system resistance measured by electrochemical impedance spectroscopy (EIS), and their effect on the electrochemical performance.

Higgins *et al.* first reported the use of a two-electrode dry-strip electrode, with a 6 × 0.9 cm dimension and a rectangular graphitic working electrode.[48] Wring *et al.* were the first to report in detail on the preparation and evaluation of screen-printed carbon based electrodes, producing a rectangular SPE composed of a 3 mm circular working electrode with a 25 × 1 mm wide connecting strip and an electrode 100 mm in length.[6] This size of the working electrode offers ease of comparison between SPE platforms and older commercially available working electrodes, such as glassy carbon, gold, and platinum disc electrodes. The authors reported that the graphitic SPE sensors displayed a resistance low enough that metal coating was not required to improve conductivity. This rectangular shape, with a circular working electrode, is the classic SPE design that has remained fairly constant in terms of the shape of the electrodes and length of the connection from the working electrode to the potentiostat and is available to purchase from numerous suppliers commercially. Consequently, in this paper, we explore the effect of changing the length of the electrical connection and its impact upon the SPEs' electrochemical and electroanalytical performance and offer our insights into how these integral electrochemical platforms should be utilized in future work.

■ EXPERIMENTAL SECTION

Chemicals. All chemicals used were of analytical grade and used as received without any further purification. All solutions were prepared with deionized water of resistivity not less than 18.2 MΩ cm. Hexaamineruthenium(III) chloride, potassium ferrocyanide, potassium ferricyanide, sodium nitrite, phosphate-buffered saline (PBS) tablets, acetic acid, lead standard for ICP-MS, and β-nicotinamide adenine dinucleotide (NADH) were purchased from Merck (Gillingham, U.K.). Potassium chloride was purchased from Fisher Scientific (Loughborough, U.K.).

Electrochemical Measurements. An Ivium Compactstat (Ivium Technologies B.V., Eindhoven, the Netherlands) was used specifically for electrochemical impedance spectroscopy (EIS) experiments. The DigiElch (v7.FD; Germany) software was used for electrochemical simulations. A μ-Autolab Type (III) potentiostat (Utrecht, the Netherlands) was used to carry out all other electrochemical measurements using a three-electrode configuration. The working electrodes used in this study are screen-printed graphitic macroelectrodes (SPEs) alongside an external Pt wire and Ag/AgCl electrode as the counter and reference electrodes, respectively, unless stated otherwise. For further experimental details, please see the Supporting Information. Where stated, the effective heterogeneous electron transfer (HET) rate constant, k^0, was determined utilizing Nicholson's[49] method for quasi-reversible systems *via* the following equation: $\psi = k^0_{eff}[(\pi DnvF)/(RT)]^{-1/2}$, where ψ is a kinetic parameter and D is the diffusion coefficient ($D = 9.1 \times 10^{-6}$ cm^2 s^{-1} for Ru$(NH_3)_6^{2+/3+}$ in 0.1 M KCl supporting electrolyte).[50,51] For further details on how these were calculated, please go to the Supporting Information.

Screen-Printed Electrode Fabrication. The SPEs comprise a three-electrode configuration with a 3.1 mm graphite working electrode, a graphite counter, and an Ag/AgCl pseudo-reference electrode. The electrodes were produced as explained in Figure 1A to produce SPEs with

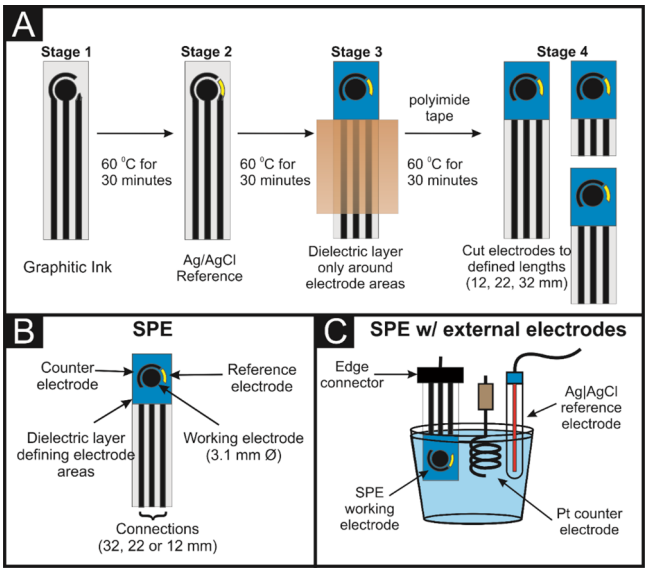

Figure 1. (A) Schematic for the production of the SPEs using polyimide tape to limit dielectric coverage and allow easy tailoring of connection length. (B) Schematic of an SPE. (C) Schematic of the three-electrode setup used throughout these experiments with an SPE working electrode, Pt wire counter electrode, and Ag/AgCl reference electrode.

five different connection lengths (32, 27, 22, 17, and 12 mm long) that are then electrically wired *via* connection to a generic edge connector that then connects to the potentiostat. Note that the largest length electrodes are the standard size of 41 mm long × 7 mm wide; however, once inserted into the edge connector, the minimum length of the connection was measured to be 32 mm. Unless stated otherwise, electro-

https://doi.org/10.1021/acs.analchem.1c03601
Anal. Chem. XXXX, XXX, XXX−XXX

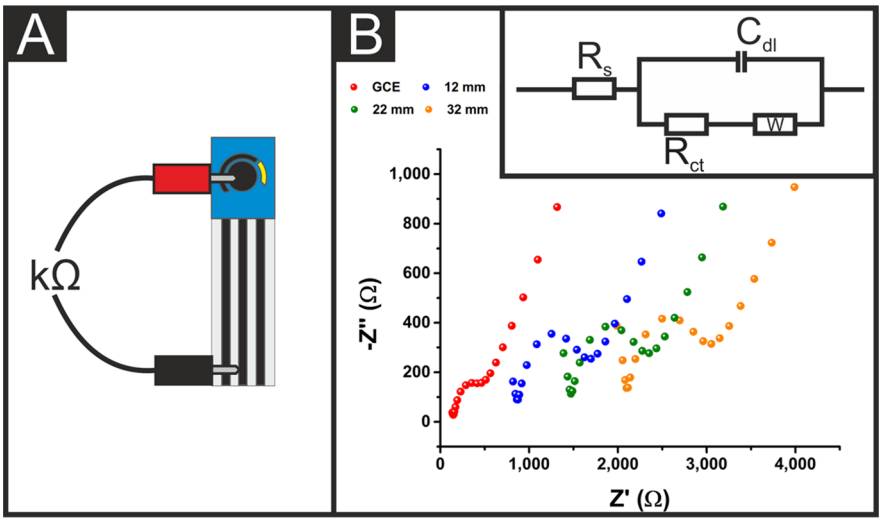

Figure 2. (A) Schematic of how resistances were measured using a multimeter setup. (B) Electrochemical impedance spectroscopy data for each SPE connection length and a glassy carbon electrode in potassium ferri/ferrocyanide (1 mM) in potassium chloride (0.1 M) from 50,000 to 1 Hz with an amplitude of 10 mV. Equivalent circuit model used for the analysis of EIS results included in B.

chemical experiments in this manuscript used an external Pt wire counter and external Ag/AgCl reference electrode. For further details about the in-house manufacture of the SPEs, please see the Supporting Information.

■ RESULTS AND DISCUSSION

Electrode Manufacture and Resistance Characterization. The fabrication methodology for the screen-printed electrodes (SPEs) with different connection lengths is described in full in the Experimental Section. Figure 1 depicts the production steps for the different SPEs used within this manuscript. Figure 1A shows the use of polyimide tape to limit the dielectric ink coverage, allowing for the shortening of the electrode to define the electrode connection length in a precise and reproducible process. This facilitated all of the SPEs used in this work to be printed from the same batch, removing any doubt that interbatch reproducibility could play a role. Figure 1B displays an overall drawing of the SPE, composed of the working, counter, and reference electrodes (WE, CE, and RE, respectively), where the WE is a disc of 3.1 mm in diameter, the dielectric layer defines the exposed areas of the graphitic/active ink, and the electrode connections vary from 12 to 32 mm of length. Figure 1C depicts the use of the SPEs in a classic three-electrode configuration, composed of the SPE and a Pt wire and Ag/AgCl as CE and RE external electrodes, respectively, to complete the circuit.

Figure 2 shows how resistance measurements are performed by using a multimeter (n = 20) along with electrochemical impedance spectroscopy (EIS, n = 5) data obtained for each SPE's connection length and a glassy carbon electrode (GCE) for comparison in potassium 1 mM ferri/ferrocyanide (0.1 M KCl) in the 1−50,000 Hz range, with an amplitude of 10 mV. The EIS model is included in Figure 2. The capacitance of each electrode was determined from cyclic voltammograms (n = 3, Figure S1) in the non-Faradaic region of hexaamineruthenium(III) chloride (RuHex, 1 mM, 0.1 M KCl). It is immediately evident that there is a significant increase in the resistance (R) from the GCE to the SPEs, with the SPEs also showing increased R values for increasing working electrode connection lengths. Table 1 summarizes the theoretical resistance (R), resistance measured with a multimeter (R_u), and resistance measured by EIS (R_c), respectively, for the 32, 27, 22, 17, and 12 mm connection lengths. We note that R_u only measures the resistance along the electrode connection length, whereas R_c will measure the resistance in the whole setup. The theoretical resistance of a given material equals its electrical resistivity (ρ) multiplied by the length (L) over which the resistance is measured, divided by the cross-sectional area of the material (A): $R = (\rho L)/A$.[52] The cross-sectional area can also be calculated by multiplying the thickness of the graphite print times the width of the connection, resulting in a cross-sectional area of 0.00128 cm^2. The calculated theoretical electrical resistance (R) for the electrodes is 2.75, 2.32, 1.89, 1.46, and 1.03 kΩ for the 32, 27, 22, 17, and 12 mm SPEs, respectively, as shown in Table 1. The averaged measured resistance values by both the multimeter, ranging from 2.33 to 0.99 kΩ, and EIS, from 2.16 to 0.90 kΩ, correlate well and follow the trend and theoretical values for the SPEs, where the shorter the graphitic connection is, the smaller the resistance is. Note that the capacitance of each electrode surface (Figure S1) shows no change as a function of the connection length of the electrode. We next turn to investigating whether this shortening of the electrode connection length, and the consequent reduction in resistance, had a significant effect on the electrochemical performance of the electrodes.

Table 1. A Summary of the Resistance between the SPE Working Electrode and the Connection Point, Measured with a Multimeter (N = 20) and with Electrochemical Impedance Spectroscopy (EIS, N = 5)

distance from working electrode (mm)	capacitance (μF) (n = 3)	theoretical resistance (R) (kΩ)	average resistance multimeter, R_u (kΩ) (n = 20)	average resistance EIS, R_c (kΩ) (n = 5)
32	0.21 ± 0.01	2.75	2.33 ± 0.13	2.16 ± 0.06
27	0.22 ± 0.01	2.32	1.99 ± 0.10	1.79 ± 0.05
22	0.21 ± 0.03	1.89	1.62 ± 0.09	1.50 ± 0.03
17	0.20 ± 0.01	1.46	1.24 ± 0.07	1.32 ± 0.03
12	0.24 ± 0.01	1.03	0.99 ± 0.04	0.90 ± 0.03

https://doi.org/10.1021/acs.analchem.1c03601
Anal. Chem. XXXX, XXX, XXX−XXX

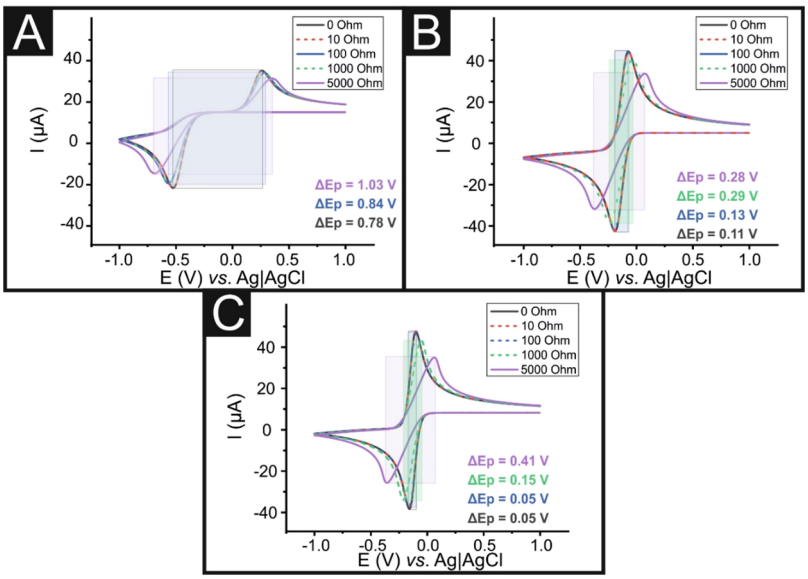

Figure 3. Simulation voltammograms for reversible (A), quasi-reversible (B), and irreversible (C) processes. Simulation parameters: $A = 0.07\ cm^2$; $\nu = 1\ V\ s^{-1}$; $T = 295$ K; $k^0 = 0.1\ cm\ s^{-1}$; $C_d = 0.21\ \mu F$; D, are equal to $9.1 \times 10^{-6}\ cm^2\ s^{-1}$; $E_f = -0.13$ V; initial concentration of A, [A], is 1 mM, initial [B] is 0 mM; $\alpha = 0.5$. $R_u = 0$, 10, 100, 1000, and 5000 Ω.

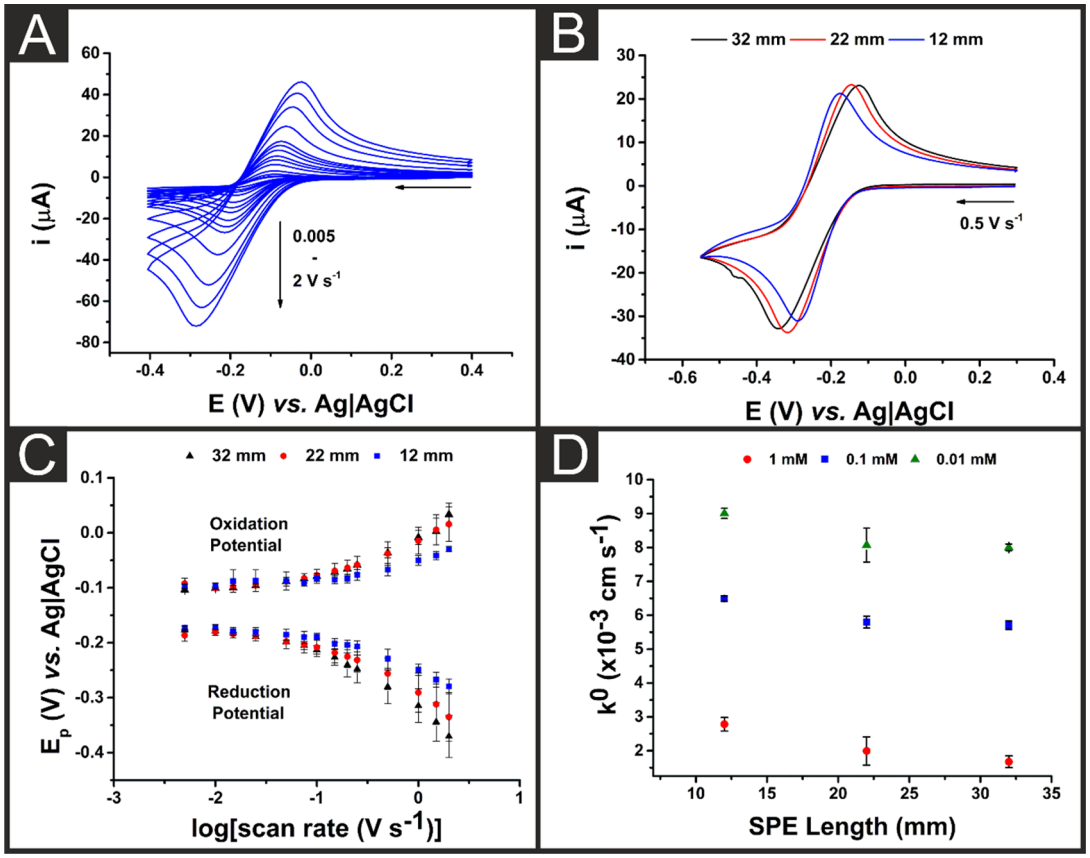

Figure 4. (A) Voltammograms corresponding to the scan rate study for a 12 mm SPE using hexaamineruthenium(III) chloride (1 mM) in potassium chloride (0.1 M) *vs* an Ag/AgCl reference electrode. (B) Voltammograms obtained at 0.5 V s^{-1} for SPEs of different connection lengths (32, 22, and 12 mm). (C) Plot of the average peak potential ($n = 3$) using SPEs of different connection lengths (32, 22, and 12 mm) *vs* the log of the scan rate for both the reduction and oxidation of hexaamineruthenium(III) chloride (1 mM) in potassium chloride (0.1 M) *vs* an Ag/AgCl reference electrode. (D) Plot of the calculated k^0 value for different connection length electrodes (32, 22, and 12 mm) using hexaamineruthenium(III) chloride (1, 0.1, and 0.01 mM) in potassium chloride (0.1 M) *vs* an Ag/AgCl reference electrode.

Electrochemistry of Different Connection Lengths of SPE Platforms. Next, we focus on the effect of the electrode resistance parameter on simulated voltammograms. The reduction current of a simple one-electron process, A + e^-

https://doi.org/10.1021/acs.analchem.1c03601
Anal. Chem. XXXX, XXX, XXX−XXX

$\rightleftharpoons B$, can be described by the following integral equation when the electron transfer is assumed as fast:

$$\frac{1}{\sqrt{\pi}}\int_0^{\tau}\frac{\psi(\eta)}{\sqrt{\tau-\eta}}d\eta=\frac{1}{1+\exp(-\xi)} \quad (1)$$

where τ, ξ, and ψ are the normalized time, potential, and current, respectively, defined by

$$\tau=\frac{F\nu}{RT}t,\ \xi=-\frac{F}{RT}(E-E^0),\ \psi=\frac{i}{FAC_{\text{bulk}}D^{1/2}\sqrt{\frac{F\nu}{RT}}}$$

where D is the diffusion coefficient assumed to the same for A and B. The above equation is modified to include the double layer charge and ohmic drop, and the current for the simple one-electron process is now governed by the following:[53]

$$\frac{1}{\sqrt{\pi}}\int_0^{\tau}\left(\psi-\frac{\Theta}{\rho}+\Theta\frac{d\psi}{d\eta}\right)\frac{\psi(\eta)}{\sqrt{\xi-\eta}}=\frac{1}{1+\exp(-\xi+\rho\psi)} \quad (2)$$

where $\rho=\frac{F}{RT}R_uFAC_{\text{bulk}}D^{1/2}\sqrt{\frac{F\nu}{RT}}$ and $\Theta=R_uC_d\frac{F\nu}{RT}$.

The effect of ohmic drop, R_u, on the cyclic voltammetric response for a simple electrochemical process, $A+e^-\rightleftharpoons B$, can be deduced via either using a digital simulation software (*e.g.*, COMSOL) or using digital simulations (DigiElch). We utilized DigiElch to explore the effect of ohmic drop, R_u, on the cyclic voltammetric response that is shown in Figure 3 following the Butler-Volmer kinetics/theory. Note that we use the classification by Matsuda and Ayabe, through the use of the parameter Λ,which is defined as[54]

$$\Lambda=\frac{k^0}{\left(\frac{FD\nu}{RT}\right)^{1/2}}$$

where $k^0$is the heterogeneous rate constant. This ensures that the electrochemical parameters correspond to reversible ($\Lambda\geq 15$), quasi-reversible ($15>\Lambda>10^{-3}$), and irreversible ($\Lambda\leq 10^{-3}$) behavior.

Figure 3 shows the simulated voltammograms with the effect of changing the ohmic drop, R_u, over the range 0, 10, 100, 1000, and 5000 Ω. What is obviously apparent is the effect of the ohmic drop on the cyclic voltammetric signature where the usual reversible response (0 Ω) is affected drastically with the peak-to-peak separation increasing and the voltammetric peak height decreasing. Note that, in these simulations, the only parameter that is changing is the ohmic drop (R_u). The effect is clearly critical if used to characterize electrochemical parameters such as heterogeneous rate constants, and if used analytically, the signal is adversely affected, which will result in lower sensitivities and higher LODs when the ohmic drop is large.

To electrochemically characterize and explore the influence of the screen-printed connection length, the near ideal outer-sphere redox probe RuHex was used. RuHex is a well-known and widely characterized redox probe that only depends on the electronic structure (DoS) of graphitic electrode materials, and therefore, its application within this manuscript will offer useful fundamental insights. For these electrochemical studies, only the 32, 22, and 12 mm SPEs were analyzed as they are the longest, medium, and shortest electrode configuration manufactured. Figure 4 depicts the voltammetric responses recorded using the 32, 22, and 12 mm SPEs toward RuHex. Figure 4A shows a full scan rate study from 0.005 to 2 V s^{-1}, scanning from +0.4 to −0.4 V *vs* Ag/AgCl. This shows the characteristic voltammetric profile of RuHex, with a clear reduction peak at ∼−0.2 to −0.3 V and subsequent oxidation peak at ∼−0.1 to 0.0 V. Figure 4B compares the different voltammograms at 0.5 V s^{-1} toward RuHex when 32, 22, and 12 mm SPEs were used, exhibiting a clear increase in the peak-to-peak separation with increasing electrode connection lengths. Figure 4C shows the averaged reduction and oxidation peak potentials for RuHex against the respective log of the scan rate, where there is a good agreement at low scan rates between the different SPE connection lengths and a divergence between the three connection lengths can be appreciated at faster ones. The described changes in the peak-to-peak separation behavior when applying high scan rates are an indicator of ohmic drop effects due to an increase of resistance between the working and the reference electrodes.[55,56] To explore the presence and/or mitigation of ohmic drop, we now turn to decreasing the conductivity of the solution by reducing the supporting electrolyte/redox probe ratio. The purpose of having a deliberately added large quantity of supporting electrolyte is to ensure that the potential drop is compressed to a 10−20 Å distance from the working electrode surface to ensure that the electron transfer between the electrode and electrolyte occurs by quantum mechanical tunneling.[57] In the experiments reported above, the supporting electrolyte−redox probe ratio was initially 100 (0.1 M of KCl divided by 1 mM RuHex).[56] Table 2 shows the calculated heterogeneous electron transfer (HET) rates (k^0) calculated at each of the electrodes using 0.01, 0.1, and 1 mM RuHex (in 0.1 M KCl for all cases), which correspond to a 10,000, 1000, and 100 KCl-to-RuHex ratio. As the concentration of RuHex is decreased, the solution resistance decreases. As is evident from inspection of Table 2, the HET values for RuHex indicate a trend in which the use of shorter SPE connection lengths correlates to an increase in the calculated k^0 values. As the ohmic drop depends on the ohmic resistance (or uncompensated resistance, R_u), which is a function of the geometry of the electrochemical cell and the conductivity of the electrolyte, the observed changes in k^0 values are likely due to the electron transfer pathway and circuit resistance decreasing when the SPE connection decreases (in comparison to larger con-

Table 2. Summary of the k^0 Values for SPEs of Different Connection Lengths (32, 22, and 12 mm) Using Hexaamineruthenium(III) Chloride (1, 0.1, and 0.01 mM) in Potassium Chloride (0.1 M) *vs* an Ag/AgCl Reference Electrode

[RuHex] (mM)	SPE connection length (mm)	k^0 ($\times10^{-3}$, cm s^{-1})
1	32	1.7 ± 0.2
1	22	2.0 ± 0.4
1	12	2.8 ± 0.2
0.1	32	5.7 ± 0.1
0.1	22	5.8 ± 0.2
0.1	12	6.5 ± 0.1
0.01	32	8.0 ± 0.1
0.01	22	8.1 ± 0.8
0.01	12	9.0 ± 0.2

https://doi.org/10.1021/acs.analchem.1c03601
Anal. Chem. XXXX, XXX, XXX−XXX

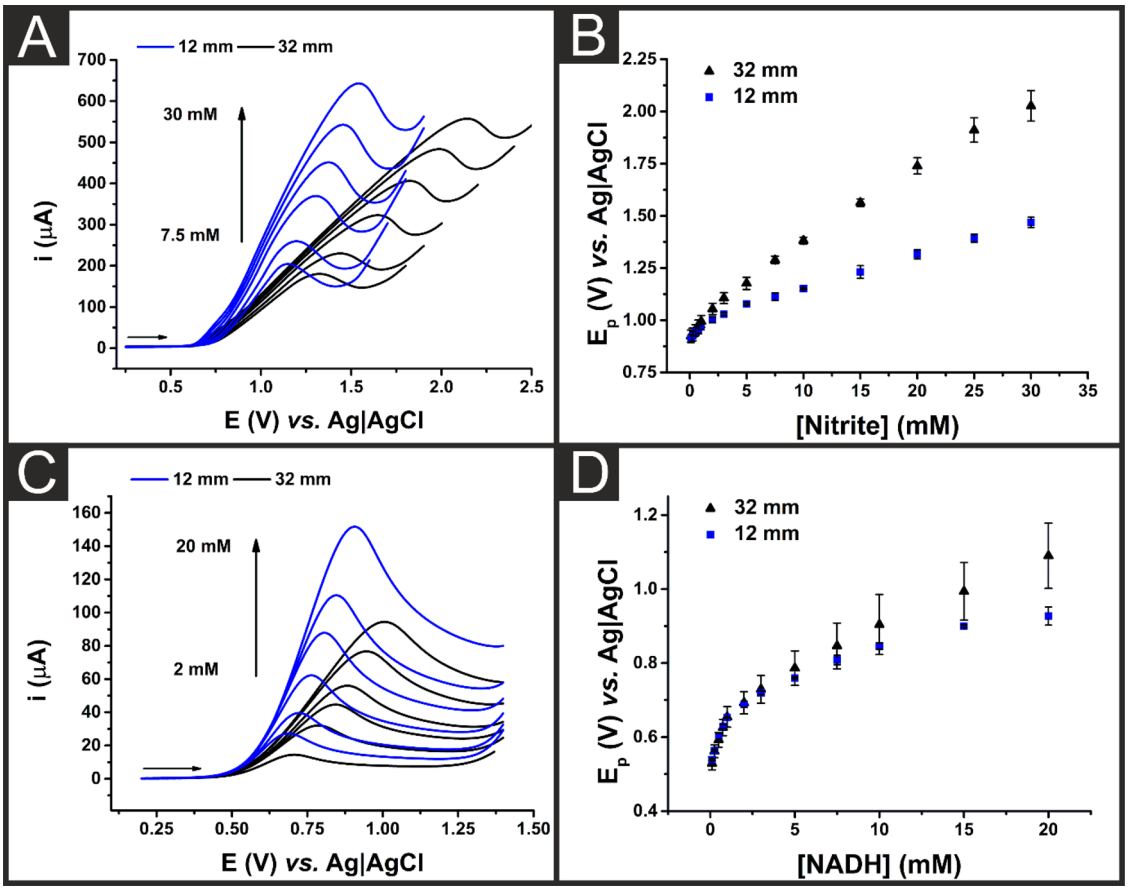

Figure 5. (A) Voltammograms corresponding to the oxidation of sodium nitrite (7.5−30 mM) in PBS (pH = 7.4) using SPEs of two different connection lengths (32 and 12 mm). (B) Plot of the average peak potential (n = 3) for the oxidation of sodium nitrite (0.1−30 mM) in PBS (pH = 7.4) using SPEs of two different connection lengths (32 and 12 mm). (C) Voltammograms corresponding to the oxidation of NADH (2−20 mM) in PBS (pH = 7.4) using SPEs of two different connection lengths (32 and 12 mm). (D) Plot of the average peak potential (n = 3) for the oxidation of NADH (0.1−20 mM) in PBS (pH = 7.4) using SPEs of two different connection lengths (32 and 12 mm).

nections). In summary, with a low solution resistance and a low electrode resistance (shortest SPE connection length), the determination of the HET becomes more accurate. This clearly has a significant implication in the electrochemical field where SPEs are utilized.

We next consider the case of using IR compensation that is offered within the software that runs most potentiostats. Figure S2 shows a comparison of RuHex voltammograms using 32 (A), 22 (B), and 12 (C) mm length connection SPEs that shows the effect of IR compensation by the software. In this case, we input the resistance measured from the EIS result into the software to realize the IR corrected cyclic voltammograms. It is clear upon their inspection that there is a small change in the voltammograms after the IR compensation. If one would want to compensate the measured resistance onto the experimental setup, the HET rate constant values, k^0, would change from 1.7, 2.0, and 2.8 × 10^{-3} cm s^{-1} to 1.8, 2.9, and 3.4 × 10^{-3} cm s^{-1} for the 32, 22, and 12 mm connection length SPEs, respectively (averaged resistance by EIS taken from Table 1; see Figure S2 voltammograms in the Supporting Information). Note that IR compensation, although useful, is often avoided by experimentalists as it has been reported to introduce undesirable effects on the recorded signals,[58] and we suggest that experiments recourse to shortened SPEs rather than IR correction.

In addition to the above and to explore if the impact of the electrode performance is due to the electrode circuit length or only the working electrode's connection length, made of graphite in this particular case, we turned to compare the peak-to-peak separation of RuHex when using an external Ag/AgCl electrode (as used above) against using a built-in pseudo-reference Ag/AgCl screen-printed electrode at different lengths. Figure S3 depicts the effect of using a built-in pseudo-reference electrode with varying lengths (32 and 12 mm) against an external Ag/AgCl. This clearly shows that when using a 32 mm length for the WE with both 32 and 12 mm printed pseudo-reference, there is good agreement in terms of their peak-to-peak separation toward RuHex. Figure S3 also shows that when using a 12 mm connection length for both WE and RE, there is indeed a significant decrease in the ΔE_p, which can only be then attributed to the graphitic working electrode connection length. Table S1 summarizes the analyzed working and reference electrode connection length combinations that were tested, with their respective HET rate constant, k^0, calculated as 2.03, 1.92, and 4.19 × 10^{-3} cm s^{-1} for the 32 mm WE and RE, 32 mm WE and 12 mm RE, and 12 mm for both WE and RE connections. We now turn to exploring the electroanalytical performance of SPEs with different connections length (32 and 12 mm) toward the electroanalytical detection of sodium nitrite, β-nicotinamide

https://doi.org/10.1021/acs.analchem.1c03601
Anal. Chem. XXXX, XXX, XXX−XXX

adenine dinucleotide (NADH), and lead (II) ions to correlate the responses based upon the SPE connection length.

Electroanalytical Performance of Different Connection Length SPE Platforms. Figure 5A,B shows the recorded voltammograms and peak potential for the electrochemical oxidation of sodium nitrite in PBS in the concentration range of 7.5−30 mM, respectively. This clearly shows a positive shift in the recorded oxidation potential with increasing concentrations of sodium nitrite for both systems, with a much greater shift shown for the longer electrode connection length. This same trend is observed in the case of NADH for both connection lengths of SPE. Figure 5C,D depicts, again, the voltammograms and peak potential data recorded for the electrochemical oxidation of NADH in the 2−20 mM range in PBS when using 32 and 12 mm SPE connection lengths. In the case of NADH, which has a lower oxidation peak potential compared to the sodium nitrite, the difference observed between the peak potentials for the different SPE connection lengths is significantly reduced. It is evident when comparing both connection lengths that when oxidating both analytes, a less positive overpotential is needed when using the 12 mm ones. It can also be seen that the average peak current for the oxidation of sodium nitrite and NADH both increase significantly when using 12 mm connection SPEs. Note that at low solution resistances, *i.e.*, in the initial region of low concentrations, the electroanalytical responses of the 32 and 12 mm SPEs converge, indicating that if only very low (trace levels) concentrations are to be determined, the effect of SPE connection lengths is negligible.

Last, the 12 and 32 mm SPEs are used as a disposable single-shot three-electrode system toward the electroanalytical sensing of lead (II) using their counter and reference built-in electrodes. Figure S4 depicts the calibration plot (peak height (current) *vs* concentration (ppb)) using the 12 and 32 mm SPE platforms as one-shot (working, counter, and reference built-in electrodes) disposable sensing devices toward lead (II) in 0.1 M acetic buffer (pH 4.5) without the use of stirring. The analysis of the SWV is found to be linear over the 4.78 to 82.824 ppb Pb^{2+} with the following linear regressions: Ip (μA) = 0.0898 μA/ppb + 2.046 μA; R^2 = 0.991 and Ip (μA) = 0.0438 μA/ppb + 1.9667 μA; R^2 = 0.994 for 12 and 32 mm SPEs, respectively (N = 6). It is clear that the same trend observed in the above manuscript, *i.e.*, the lower resistance of the 12 mm SPE, is translated into a higher analytical sensitivity when shorter SPE connection lengths are used toward lead (II) sensing compared to the responses obtained when using "relatively" larger SPEs. All of these data point to an improved electrochemical performance by the SPE of shorter connection length. In the future, we note that it is important to include the connection lengths or resistance of the SPEs in published work to bring simplicity in the comparison between different reports.

CONCLUSIONS

This manuscript shows the crucial relationship between the *heterogeneous electron transfer (HET) rate* (k^0) values and the graphite screen-printed electrode dimensions. It is reported herein that there is a difference between the k^0 values obtained at different SPE connection lengths due to the changing resistance, which is directly related to its connection length. It has also been demonstrated that such difference is also exhibited when explored toward the electroanalytical determination of sodium nitrite, NADH, and lead (II) ions. We have shown herein that the resistance changes due to SPE connection length cannot be overcome by IR compensation; however, we are reporting a clear benefit when using SPEs with graphitic connections of shorter lengths. These findings are of high importance to those experimentalists working with screen-printed electrode sensors, particularly to those designing their own SPE platforms. The observations described in this manuscript highlight the impact and relevance of reporting the working electrode's resistance by electrochemical impedance spectroscopy (EIS) and/or a multimeter reading for benchmarking purposes.

ASSOCIATED CONTENT

Supporting Information

The Supporting Information is available free of charge at https://pubs.acs.org/doi/10.1021/acs.analchem.1c03601.

Additional experimental details, including the electrochemical procedures and SPE manufacturing process; Table S1 and Figures S1−S4 showing the capacitance calculations, IR compensation, pseudo-reference, and lead determination experiments, respectively (PDF)

AUTHOR INFORMATION

Corresponding Author

Craig E Banks − *Faculty of Science and Engineering, Manchester Metropolitan University, Manchester M1 5GD, U.K.*; orcid.org/0000-0002-0756-9764; Phone: ++(0) 1612471196; Email: c.banks@mmu.ac.uk

Authors

Matthew J. Whittingham − *Faculty of Science and Engineering, Manchester Metropolitan University, Manchester M1 5GD, U.K.*

Nicholas J. Hurst − *Faculty of Science and Engineering, Manchester Metropolitan University, Manchester M1 5GD, U.K.*

Robert D. Crapnell − *Faculty of Science and Engineering, Manchester Metropolitan University, Manchester M1 5GD, U.K.*

Alejandro Garcia-Miranda Ferrari − *Faculty of Science and Engineering, Manchester Metropolitan University, Manchester M1 5GD, U.K.*; orcid.org/0000-0003-1797-1519

Elias Blanco − *Faculty of Science and Engineering, Manchester Metropolitan University, Manchester M1 5GD, U.K.; Departamento de Química Analítica y Análisis Instrumental, Facultad de Ciencias, Universidad Autónoma de Madrid, Madrid 28049, Spain*; orcid.org/0000-0003-0042-6266

Trevor J. Davies − *Electrochemical Technology Technical Centre, INOVYN, Cheshire WA7 4JE, U.K.*

Complete contact information is available at: https://pubs.acs.org/10.1021/acs.analchem.1c03601

Notes

The authors declare no competing financial interest.

ACKNOWLEDGMENTS

Funding from the Engineering and Physical Sciences Research Council (Reference: EP/P007767/1 and EP/N0011877/1) is acknowledged. A.G.-M.F. would like to acknowledge Innovate U.K. for funding his Knowledge Transfer Partnership (KTP Reference: 11606). We thank C.W. Foster for initial experimental investigations.

REFERENCES

(1) Mannino, S.; Wang, J. *Electroanalysis* **1992**, *4*, 835−840.
(2) Brainina, K.; Henze, G.; Stojko, N.; Malakhova, N.; Faller, C. *Fresenius' J. Anal. Chem.* **1999**, *364*, 285−295.
(3) Brainina, K. Z. *J. Anal. Chem.* **2001**, *56*, 303−312.
(4) Niu, X.; Lan, M.; Zhao, H.; Chen, C.; Li, Y.; Zhu, X. *Anal. Lett.* **2013**, *46*, 2479−2502.
(5) Ferrari, A. G.-M.; Rowley-Neale, S. J.; Banks, C. E. *Talanta Open* **2021**, *3*, 100032.
(6) Wring, S. A.; Hart, J. P.; Bracey, L.; Birch, B. J. *Anal. Chim. Acta* **1990**, *231*, 203−212.
(7) Squissato, A. L.; Munoz, R. A. A.; Banks, C. E.; Richter, E. M. *ChemElectroChem* **2020**, *7*, 2211−2221.
(8) Smart, A.; Crew, A.; Pemberton, R.; Hughes, G.; Doran, O.; Hart, J. P. *TrAC Trends Anal. Chem.* **2020**, *127*, 115898.
(9) Wang, J.; Tian, B.; Nascimento, V. B.; Angnes, L. *Electrochim. Acta* **1998**, *43*, 3459−3465.
(10) Hughes, G.; Westmacott, K.; Honeychurch, K. C.; Crew, A. P.; Pemberton, R.; Hart, J. *Biosensors* **2016**, *6*, 50.
(11) Metters, J. P.; Kadara, R. O.; Banks, C. E. *Analyst* **2011**, *136*, 1067−1076.
(12) Renedo, O. D.; Alonso-Lomillo, M. A.; Martínez, M. J. A. *Talanta* **2007**, *73*, 202−219.
(13) Metters, J. P.; Tan, F.; Kadara, R. O.; Banks, C. E. *Anal. Methods* **2012**, *4*, 1272−1277.
(14) Yu, C. Y.; Ang, G. Y.; Chan, K. G.; Banga Singh, K. K.; Chan, Y. Y. *Biosens. Bioelectron.* **2015**, *70*, 282−288.
(15) Wang, J.; Tian, B. *Anal. Chem.* **1993**, *65*, 1529−1532.
(16) Metters, J. P.; Tan, F.; Banks, C. E. *J. Solid State Electrochem.* **2013**, *17*, 1553−1562.
(17) Choudhry, N. A.; Kampouris, D. K.; Kadara, R. O.; Jenkinson, N.; Banks, C. E. *Anal. Methods* **2009**, *1*, 183−187.
(18) Zen, J.-M.; Song, Y.-S.; Chung, H.-H.; Hsu, C.-T.; Senthil Kumar, A. *Anal. Chem.* **2002**, *74*, 6126−6130.
(19) Lee, J.; Murugappan, K.; Arrigan, D. W. M.; Silvester, D. S. *Electrochim. Acta* **2013**, *101*, 158−168.
(20) Wang, J.; Musameh, M. *Analyst* **2004**, *129*, 1−2.
(21) Randviir, E. P.; Brownson, D. A. C.; Metters, J. P.; Kadara, R. O.; Banks, C. E. *Phys. Chem. Chem. Phys.* **2014**, *16*, 4598−4611.
(22) Rowley-Neale, S. J.; Brownson, D. A. C.; Smith, G.; Banks, C. E. *Biosensors* **2020**, *10*, 27.
(23) Kadara, R. O.; Jenkinson, N.; Banks, C. E. *Electroanalysis* **2009**, *21*, 2410−2414.
(24) Metters, J. P.; Kadara, R. O.; Banks, C. E. *Analyst* **2013**, *138*, 2516−2521.
(25) Craston, D. H.; Jones, C. P.; Williams, D. E.; El Murr, N. *Talanta* **1991**, *38*, 17−26.
(26) Authier, L.; Grossiord, C.; Brossier, P.; Limoges, B. *Anal. Chem.* **2001**, *73*, 4450−4456.
(27) René, A.; Cugnet, C.; Hauchard, D.; Authier, L. *Analyst* **2013**, *138*, 2192−2198.
(28) Vagin, M. Y.; Sekretaryova, A. N.; Reategui, R. S.; Lundstrom, I.; Winquist, F.; Eriksson, M. *ChemElectroChem* **2014**, *1*, 755−762.
(29) Jones, A. L.; Dhanapala, L.; Baldo, T. A.; Sharafeldin, M.; Krause, C. E.; Shen, M.; Moghaddam, S.; Faria, R. C.; Dey, D. K.; Watson, R. W.; Andrawis, R.; Lee, N. H.; Rusling, J. F. *Anal. Chem.* **2021**, 1059.
(30) Liébana, S.; Jones, L. J.; Drago, G. A.; Pittson, R. W.; Liu, D.; Perrie, W.; Hart, J. P. *Sens. Actuators, B* **2016**, *231*, 384−392.
(31) Metters, J. P.; Randviir, E. P.; Banks, C. E. *Analyst* **2014**, *139*, 5339−5349.
(32) Hallam, P. M.; Kampouris, D. K.; Kadara, R. O.; Banks, C. E. *Analyst* **2010**, *135*, 1947−1952.
(33) Metters, J. P.; Kadara, R. O.; Banks, C. E. *Analyst* **2012**, *137*, 896−902.
(34) Rana, S.; Mittal, S. K.; Singh, N.; Singh, J.; Banks, C. E. *Sens. Actuators, B* **2017**, *239*, 17−27.
(35) Khairy, M.; Ayoub, H. A.; Banks, C. E. *Food Chem.* **2018**, *255*, 104−111.
(36) Pierini, G. D.; Maccio, S. A.; Robledo, S. N.; Ferrari, A. G.-M.; Banks, C. E.; Fernández, H.; Zon, M. A. *Microchem. J.* **2020**, *159*, 105442.
(37) Gogola, J. L.; Martins, G.; Gevaerd, A.; Blanes, L.; Cardoso, J.; Marchini, F. K.; Banks, C. E.; Bergamini, M. F.; Marcolino-Junior, L. H. *Anal. Chim. Acta* **2021**, *1166*, 338548.
(38) Gómez-Mingot, M.; Iniesta, J.; Montiel, V.; Kadara, R. O.; Banks, C. E. *Analyst* **2011**, *136*, 2146−2150.
(39) Gómez-Mingot, M.; Montiel, V.; Banks, C. E.; Iniesta, J. *Analyst* **2014**, *139*, 1442−1448.
(40) Betlem, K.; Mahmood, I.; Seixas, R.; Sadiki, I.; Raimbault, R.; Foster, C.; Crapnell, R.; Tedesco, S.; Banks, C.; Gruber, J.; Peeters, M. *Chem. Eng. J.* **2019**, *359*, 505−517.
(41) Crapnell, R. D.; Jesadabundit, W.; García-Miranda Ferrari, A.; Dempsey-Hibbert, N. C.; Peeters, M.; Tridente, A.; Chailapakul, O.; Banks, C. E. *Anal. Chem.* **2021**, 5931.
(42) Jamieson, O.; Soares, T. C.; de Faria, B. A.; Hudson, A.; Mecozzi, F.; Rowley-Neale, S. J.; Banks, C. E.; Gruber, J.; Novakovic, K.; Peeters, M.; Crapnell, R. D. *Chemosensors* **2020**, *8*, 5.
(43) Jamieson, O.; Betlem, K.; Mansouri, N.; Crapnell, R. D.; Vieira, F. S.; Hudson, A.; Banks, C. E.; Liauw, C. M.; Gruber, J.; Zubko, M.; Whitehead, K. A.; Peeters, M. *Therm. Sci. Eng. Prog.* **2021**, *24*, 100956.
(44) McClements, J.; Seumo Tchekwagep, P. M.; Vilela Strapazon, A. L.; Canfarotta, F.; Thomson, A.; Czulak, J.; Johnson, R. E.; Novakovic, K.; Losada-Pérez, P.; Zaman, A.; Spyridopoulos, I.; Crapnell, R. D.; Banks, C. E.; Peeters, M. *ACS Appl. Mater. Int.* **2021**, 27868.
(45) Costentin, C.; Savéant, J.-M. *Energy Storage Mater.* **2020**, *24*, 1−3.
(46) Sillanpää, M.; Shestakova, M., Chapter 1 - Introduction. In *Electrochemical Water Treatment Methods*; Sillanpää, M.; Shestakova, M., Eds. Butterworth-Heinemann: 2017; pp. 1−46, DOI: 10.1016/B978-0-12-811462-9.00001-3.
(47) Bard, A.; Faulkner, L., *Electrochemical Methods: Fundamentals and Applications*; John Wiley & Sons, Inc: 2001.
(48) Higgins, I. J.; McCann, J. M.; Davis, G.; Hill, H. A. O.; Zwansiger, R.; Treidl, B. L.; Birket, N. N.; Plotkin, E. V. *Eur. Pat. Appl.* **1984**, *127*, 958.
(49) Nicholson, R. S. *Anal. Chem.* **1965**, *37*, 1351−1355.
(50) García-Miranda Ferrari, A.; Foster, C.; Kelly, P.; Brownson, D.; Banks, C. Determination of the Electrochemical Area of Screen-Printed Electrochemical Sensing Platforms. *Biosensors* **2018**, *8* (), DOI: 10.3390/bios8020053.
(51) Wang, Y.; Limon-Petersen, J. G.; Compton, R. G. *J. Electroanal. Chem.* **2011**, *652*, 13−17.
(52) Woolf, L. D.; Streckert, H. H. *Phys. Teach.* **1996**, *34*, 440−441.
(53) Imbeaux, J. C.; Savéant, J. M. *J. Electroanal. Chem. Int. Electrochem.* **1970**, *28*, 325−338.
(54) Matsuda, H.; Ayabe, Y. *Z. Elektrochem. angew. phys. Chem.* **1955**, *59*, 494−503.
(55) Savéant, J.-M. *Elements of Molecular and Biomolecular Electrochemistry*; John Wiley Sons: 2006.
(56) Elgrishi, N.; Rountree, K. J.; McCarthy, B. D.; Rountree, E. S.; Eisenhart, T. T.; Dempsey, J. L. *J. Chem. Educ.* **2018**, *95*, 197−206.
(57) Compton, R. G.; Banks, C. E. *Understanding Voltammetry*. 2nd ed.; Imperial College Press: 2010.
(58) Britz, D.; Strutwolf, J., Britz, D.; Strutwolf, J. Effects Due to Uncompensated Resistance and Capacitance. In *Digital Simulation in Electrochemistry*; Britz, D.; Strutwolf, J., Eds. Springer International Publishing: Cham, 2016; pp. 241−249, DOI: 10.1007/978-3-319-30292-8_11.

https://doi.org/10.1021/acs.analchem.1c03601
Anal. Chem. XXXX, XXX, XXX−XXX